
DLME: DEEP LOCAL-FLATNESS MANIFOLD EMBEDDING ^{*}

Zelin Zang^{*}, Siyuan Li^{*}, Di Wu, Ge Wang, Stan Z. Li[†]
Zhejiang University,
Westlake University, AI Lab, School of Engineering
Hangzhou, 310000, China
{zangzelin, stan.zq.li}@westlake.edu.cn

Lei Shang, Baigui Sun, Hao Li,
Alibaba Group
Hangzhou, China

ABSTRACT

Manifold learning (ML) aims to find low-dimensional embedding from high-dimensional data. Previous works focus on handcraft or easy datasets with simple and ideal scenarios; however, we find they perform poorly on real-world datasets with under-sampling data. Generally, ML methods primarily model data structure and subsequently process a low-dimensional embedding, where the poor local connectivity of under-sampling data in the former step and inappropriate optimization objectives in the later step will lead to *structural distortion* and *underconstrained embedding*. To solve this problem, we propose Deep Local-flatness Manifold Embedding (DLME), a novel ML framework to obtain reliable manifold embedding by reducing distortion. Our proposed DLME constructs semantic manifolds by data augmentation and overcomes *structural distortion* problems with the help of its smooth framework. To overcome *underconstrained embedding*, we design a specific loss for DLME and mathematically demonstrate that it leads to a more suitable embedding based on our proposed Local Flatness Assumption. In the experiments, by showing the effectiveness of DLME on downstream classification, clustering, and visualization tasks with three types of datasets (toy, biological, and image), our experimental results show that DLME outperforms SOTA ML & contrastive learning (CL) methods.

Keywords Manifold Learning · Deep Learning · Local Flatness Assumption of Manifold

1 Introduction

The intrinsic dimension of high-dimensional data is usually much lower and how to effectively learn a low-dimensional representation is a fundamental problem in traditional machine learning [1], data mining [2], and pattern recognition [3]. Manifold learning (ML), based on solid mathematical foundations and assumptions, discusses manifold representation problems under unsupervised conditions and has a far-reaching impact. However, the application of the manifold learning method is limited, and we attribute the reasons to the following two reasons: **(D1) Underconstrained manifold embedding**. ML methods focus on local relationships, while it is prone to distorted embeddings that affect the performance of downstream tasks (in Fig. 2 (D2) and Fig. 6). Paper [4, 5] suggests even the most advanced ML methods lose performance on downstream tasks due to inadequate constraints on the latent space. We attribute the reason to the limitations of traditional ML methods based on similarity/dissimilarity loss function design. **(D2) Structural distortion**. ML methods focus on handcraft or easy datasets and are not satisfactory in handling real-world datasets. We attribute the problem to **structural distortion**: The ML approach uses the distances in the input space to construct locally connected graphs and defines structure-preserving unsupervised learning loss functions [6, 7]. However, the above loss function introduces a stringent assumption: the local connectivity assumption (LCA). This assumption suggests that the distance metric of the data can describe the neighbor relationship of the data, which is often only possible if the data are densely sampled. LCA is not easily guaranteed in the real world, e.g., pictures of two dogs are not necessarily similar in terms of pixel metric (in Fig. 2 (D2)).

Meanwhile, Contrastive Learning (CL) is enthusiastically discussed in the image and NLP fields [8, 9, 10]. These methods have shown excellent performance by introducing prior knowledge of the data with the help of data augmenta-

^{**} Equal contribution, [†] Corresponding author

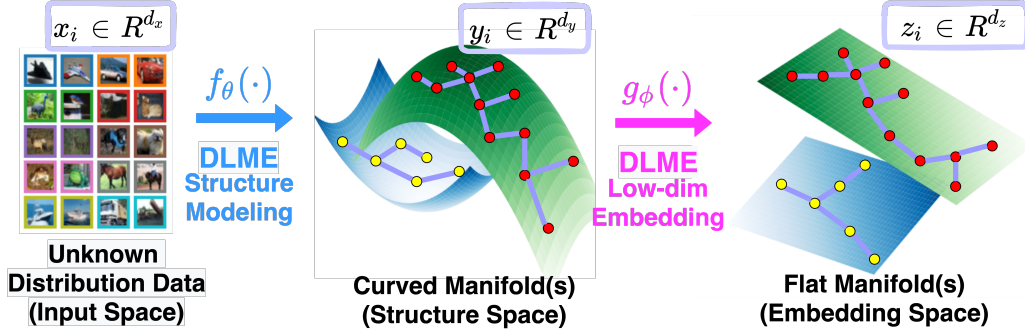


Figure 1: DLME includes the structure modeling network $f_\theta(\cdot)$ and low-dim embedding network $g_\phi(\cdot)$. The $f_\theta(\cdot)$ maps the input data into structure space to describe the data relationship. The $g_\phi(\cdot)$ maps the curled manifold into the flat embedding space to improve the discriminative performance and friendliness to downstream tasks. $f_\theta(\cdot)$ and $g_\phi(\cdot)$ are compatible with any neural network.

tion. However, we have encountered more significant difficulties applying such methods to the ML domain. The above methods require a large amount of data for pre-training [11, 12], so it is not easy to achieve good results in areas where data is expensive (e.g., biology, medicine, etc.). We consider that the core issues can be summarized as: **(D3) Local collapse embedding**. The unsmoothed loss of the CL leads to the model that is prone to local collapse and requires a large diversity of data to learn valid knowledge (in Fig. 1 (D3)).

We want to propose a new deep ML model that can better constrain the latent space and solve the structural distortion problem with the data augmentation of CL. At the same time, we hope that the proposed method can avoid the local collapse phenomenon in the CL method. We started from the ML perspective and divided the process into two sub-processes: (a) *structural modeling*: obtains the graph structures of data manifolds by measuring the relationship of each sample pair which serves as the guidance for low-dimensional embedding. (b) *low-dimensional embedding*: mapping the provided structures into the embedding space.

We propose a novel deep ML framework named deep local-flatness manifold embedding (DLME) to solve both problems by merging the advantages of ML and CL. We firstly propose a novel local flatness assumption (LFA) to obtain a more reasonable latent space by adding a second-order manifold curvature constraint (for **D1**); thus improving the performance of the method on downstream tasks. We then designed a new neural network framework that is compatible with data augmentation and can be more easily trained and generalized for use (for **D2**). DLME framework accomplishes the two sub-processes with two networks ($f_\theta(\cdot)$ and $g_\phi(\cdot)$) optimized by the proposed DLME loss between the latent space of $f_\theta(\cdot)$ and $g_\phi(\cdot)$ in an end-to-end manner (framework is in Fig. 1). We then design a smoothing loss function compatible with data augmentation based on the local flatness assumption. The loss function is based on a long-tailed t-distribution and guides the network learning through the two latent spaces (for **D3**). Finally, we further illustrate mathematically: (1) the differences between DLME loss and conventional CL loss, and (2) why DLME loss can obtain a locally flat embedding.

In short, this work makes the following contributions:

- We provide a novel deep ML framework that utilizes neural networks instead of distance metrics in data space (e.g., kNN) to better model structural relationships, thus overcoming structural distortions.
- We put forward the concept of local flatness of manifolds and theoretically discuss that the DLME loss can enhance the flatness of manifolds and obtain transfer abilities to downstream tasks, thus overcoming underconstrained manifold embedding.
- We demonstrate the effectiveness of DLME on three downstream tasks with three types of datasets (toy, biological, and image), and experiments results show that DLME outperforms current state-of-the-art ML and CL methods.

2 Related Works

In **manifold learning**, MDS [13], ISOMAP [14], and LLE [15] model the structure of data manifolds based on local or global distances (dissimilarity) and linearly project to the low-dimensional space. SNE [16], t-SNE [7] and UMAP [6] use normal distribution to define local similarities and apply the Gaussian or t-distribution kernel to transform the

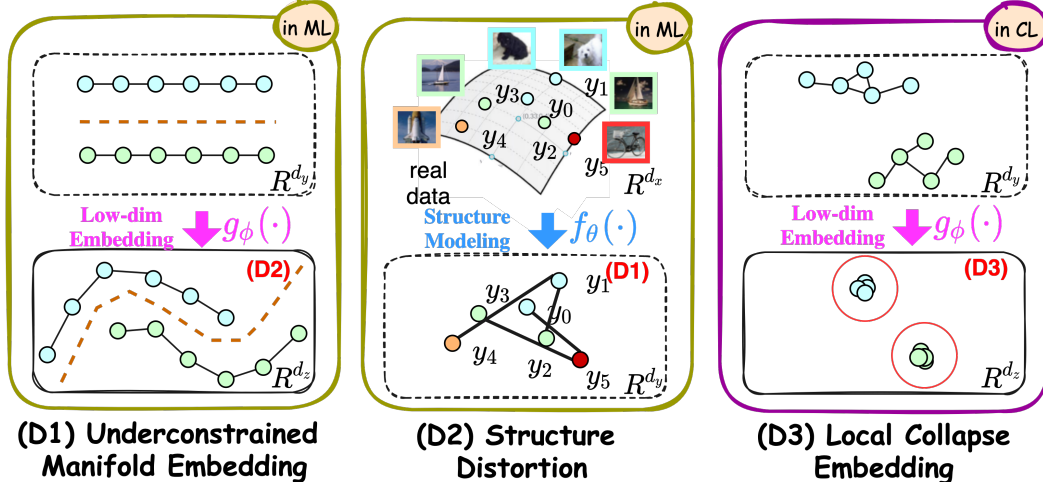


Figure 2: Problems in ML and CL. **(D1)** Local field of view & first-order (similarity/dissimilarity) constraints \rightarrow underconstrained manifold embedding. **(D2)** complexity of real-world data (ultra-high dimensionality or non well-sampling) \rightarrow broke the local connectivity of manifold \rightarrow structure distortions. **(D3)** unsmoothed losses function \rightarrow local collapse embedding.

distance into the pair-wise similarity for *structural modeling*. They perform the manifold embedding by preserving the local geometric structures explored from the input data.

In **deep manifold learning**, Parametric t-SNE (P-TSNE) [17] and Parametric UMAP [18] learn more complex manifolds by non-linear neural networks and can transfer to unseen data. However, they inherit the original *structural modeling* strategies in t-SNE and UMAP. Topological autoencoder (TAE), Geometry Regularized AutoEncoders (GRAE) [19], and ivis [20] abandon the accurate modeling of input data and directly achieve *low-dimensional embedding* using distances or contrast training.

In **self-supervised contrastive learning**, contrastive-based methods [21, 8, 9, 10] which learns instance-level discriminative representations by contrasting positive and negative views have largely reduced the performance gap between supervised models on various downstream tasks. Deep clustering methods is another popular form of self-supervised pretraining. We provide a more detailed comparison in Appendix.

3 Methods

3.1 Problem Description and Local Flatness Assumptions

This section introduces the local flatness assumption (LFA) and describes the theoretical and practical implications. According to Nash embedding theorems [22], we mainly discuss manifolds represented in Euclidean coordinates and provide the definitions of manifold learning (ML) and deep manifold learning (DML) in practical scenarios.

Definition 1 (Manifold Learning, ML). Let \mathcal{M} be a d -dimensional embedding in Euclidean space \mathbb{R}^d and $f : \mathcal{M} \rightarrow \mathbb{R}^D$ be a diffeomorphic embedding map, for $D > d$, the purpose of manifold learning is to find $\{z_i\}_{i=1}^N, z_i \in \mathcal{M}$ from the sufficient sampled (observed) data $X = \{x_i\}_{i=1}^N, x_i \in \mathbb{R}^D$.

Based on Definition 1, we define deep manifold learning (DML) as finding the embedding $\{z_i\}_{i=1}^N, z_i \in \mathcal{M}$ by the mapping $g_\theta : \mathbb{R}^D \rightarrow \mathbb{R}^d$ with the neural network parameters θ .

Each ML method designs a loss function based on the specific manifold assumption to map the observed data $\{x_i\}$ back to the intrinsic manifold $\{z_i\}$. For example, LLE [23] assumes that the local manifold is linear, and UMAP [6] assumes that the local manifold is uniform. We propose a very different assumption, considering the nature of the manifold in the latent space from the local flatness.

Assumptions 1 (Local Flatness Assumption, LFA). Let \mathcal{M} be a manifold, and $\{x_i\}$ be a set of observations in the manifold. We expect each data point and its neighbors to lie on or close to a local flatness patch. To quantitate the flatness, we introduce Gauss-Bonnet theorem [24], and use the mean curvature $\bar{K}_{\mathcal{M}}$ to quantify the flatness of

high-dimensional manifolds:

$$\begin{aligned} \bar{K}_{\mathcal{M}} &= \sum_{x_i \in X} k(x_i) \\ k(x_i) &= 2\pi\chi(\mathcal{M}) - \theta(x_{|H_1(x_i)|}, x_i, x_0) - \sum_{j \in \{0, 1, \dots, |H_1(x_i)|-1\}} \theta(x_j, x_i, x_{j+1}) \end{aligned} \quad (1)$$

where $\chi(\mathcal{M})$ is Euler Characteristic [25]. $H_1(x_i)$ is the hop-1 neighbor of x_i . $\theta(x_i, x_j, x_k)$ is the angle of three point x_i, x_j, x_k .

From first-order constraint to second-order (curvature) constraint. ML methods (e.g., LLE and UMAP) design distance-preserving or similarity-preserving objective functions, hoping to guarantee the first-order relationship of the data during the flow mapping process. However, first-order relation preservation is not a tight constraint when the local structure of the manifold is simple, which is an important cause of underconstrained manifold embedding in ML. We introduce a second-order (curvature) constraint to solve the distortion problem. Due to the expensive complexity of second-order losses, we directly minimize the curvature of the manifold by a mundane flatness assumption. Such an idea is similar to the sparsity prior in Compressed sensing (also called compressive sampling) [26], where the local flatness assumption expects the local curvature information that is not tightly constrained to be sparse.

Empirical benefits of LFA. As with all ML or CL methods, LFA comes from the assumption of latent space, although we believe it is beneficial for a variety of downstream tasks. For the single-manifold case, the assumption of ‘Local Flatness’ reduces curling in the unsuitable embedding space (see Fig. 6), thus avoiding distortion during embedding. For the multi-manifolds case, assuming ‘Local Flatness’ can simplify the discriminative relations of multi-manifolds. While avoiding collapse, our assumption also reduces the possibility of different manifolds overlapping, ultimately making the downstream task easy to be accomplished by a simple linear model.

3.2 DLME Framework

The DLME framework (in Fig. 3) contains two neural networks (f_θ and g_ϕ) and a DLME loss function L_D . The network f_θ achieves *structural modeling* in its structure space \mathbb{R}^{d_y} , and the network g_ϕ learns *low-dimensional embedding* in the embedding space \mathbb{R}^{d_z} . The DLME loss is calculated based on the A_{ij} and the pairwise similarity in spaces \mathbb{R}^{d_y} and \mathbb{R}^{d_z} used to train two neural networks from scratch. The A_{ij} indicate the homologous relationships, if x_i and x_j are augmentations of the same original data, then $A_{ij} = 1$ else $A_{ij} = 0$.

Data augmentation for solving structural distortion. ML methods have difficulty efficiently identifying neighboring nodes, causing structural distortions, when dealing with complex and not well-sampled data. DLME solves this problem with a priori knowledge provided by data augmentation. Data augmentation schemes have been widely used in self-supervised contrastive learning (CL) to solve problems in CV and NLP. From the ML perspective, data augmentation is a technique to make new observations in the intrinsic manifold based on prior knowledge. Since data augmentation changes the semantics of the original data as little as possible, it generates specific neighborhood data for each isolated data when the local connectivity of ML data is broken. DLME trains a neural network $f_\theta(\cdot)$. The $f_\theta(\cdot)$ is guided by data augmentation and loss functions to map the data into a latent space that better guarantees local connectivity.

Data augmentation is designed based on domain knowledge. For example, in CV datasets, operations such as color jittering [27], random cropping [28], applying Gaussian blur [29] are proven means. In biology and some easy datasets, linear combinations $\tau_{lc}(\cdot)$ in k-nearest neighbor data is a simple and effective way:

$$\tau_{lc}(X) = rX + (1-r)n, n \sim \text{KNN}(X) \quad (2)$$

where n is sampled from KNN. and $r \in [0, 1]$ is a combination parameter. For special domain data, the prior knowledge in the domain can be used to establish data augmentation.

The forward propagation of DLME is,

$$\begin{aligned} y_i &= f_\theta(x_i), y_i \in \mathbb{R}^{d_y}, x_i \sim \tau(X), x_j \sim \tau(X) \\ z_i &= g_\phi(y_i), z_i \in \mathbb{R}^{d_z}, d_z < d_y. \end{aligned} \quad (3)$$

where x_i and x_j sampled form different random augmentation of raw data X , the d_y and d_z are the dimension number of \mathbb{R}^{d_y} and \mathbb{R}^{d_z} .

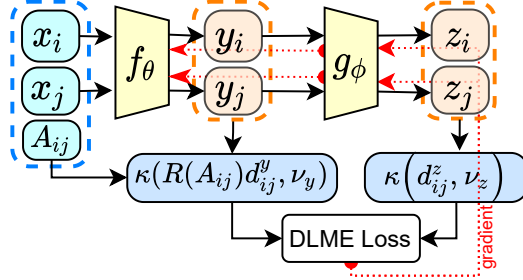


Figure 3: The framework of DLME. (x_i, x_j) is a pair of input sample, and the neighbor relationship A_{ij} indicates whether x_i and x_j are homologous pairs. The red dashed line marks the direction of the gradient back-propagation.

The loss function of DLME is,

$$L_D = E_{x_i, x_j} \left[\mathcal{D} \left(\kappa \left(R(A_{ij}) d_{ij}^y, \nu_y \right), \kappa \left(d_{ij}^z, \nu_z \right) \right) \right] \quad (4)$$

$$d_{ij}^y = d(y_i, y_j), d_{ij}^z = d(z_i, z_j)$$

d_{ij}^y and d_{ij}^z are the distance metrics of data node i and j in spaces \mathbb{R}^{d_y} and \mathbb{R}^{d_z} . The Definition of two way $\mathcal{D}(\cdot)$, kernel function $\kappa(\cdot)$, and scaling functions $R(\cdot)$ are in Eq.(5), Eq.(6) and Eq.(7).

We adopt two-way divergence [30] $\mathcal{D}(p, q)$ to measure the dis-similarity between two latent spaces,

$$\mathcal{D}(p, q) = p \log q + (1 - p) \log(1 - q), \quad (5)$$

where $p \in [0, 1]$. Notice that $\mathcal{D}(p, q)$ is a continuous version of the cross-entropy loss. In DLME, Eq. (5) is used to guide the pairwise similarity of two latent spaces to fit each other. The effect of the loss function on the two networks will be discussed in Sec 3.3 and Sec 3.4.

Due to the different latent space dimensions, there is a dimensional barrier to directly calculating the latent space distance. We adopt the t -distribution as kernel function to calculate the pairwise similarity between points to describe the data distribution. The different degrees of freedom ν_y and ν_z in t -distribution is the essential settings to enhance the flatness of embedding space (in Sec 3.4).

$$\kappa(d, \nu) = \frac{\text{Gam} \left(\frac{\nu+1}{2} \right)}{\sqrt{\nu\pi} \text{Gam} \left(\frac{\nu}{2} \right)} \left(1 + \frac{d^2}{\nu} \right)^{-\frac{\nu+1}{2}}, \quad (6)$$

where $\text{Gam}(\cdot)$ is the Gamma function, and the degrees of freedom ν controls the shape of the kernel function.

DLME design $R(A_{ij})$ to integrate the neighborhood information in A_{ij} .

$$R(A_{ij}) = 1 + (\alpha - 1)A_{ij} = \begin{cases} \alpha & \text{if } A_{ij} = 1 \\ 1 & \text{otherwise} \end{cases}, \quad (7)$$

where $\alpha \in [0, 1]$ is a hyperparameters. If x_i is the neighbor of x_j , the distance in *structure space* will be reduced by α , and the similarity of x_i and x_j will increase.

3.3 Against Local Collapse by a Smoother CL Framework

In this section we show that the DLME architecture is smoother than the CL architecture and can combat local collapse. The CL loss in self-supervised contrastive learning (CL) frameworks is

$$L_C = -\mathbb{E}_{x_i, x_j} \left[A_{ij} \log \kappa(d_{ij}^z) + (1 - A_{ij}) \log(1 - \kappa(d_{ij}^z)) \right], \quad (8)$$

where similarity kernel function $\kappa(d_{ij}^z)$ is defined in Eq.(6). The CL is not smooth and can be analogous to bang-bang control [31] in control systems. Because the learning target of the point pair will switch between $\log \kappa(d_{ij}^z)$ and $\log(1 - \kappa(d_{ij}^z))$ with the change of A_{ij} .

The proposed framework is a smoother CL framework because DLME compromises the learning process and avoids sharp conflicts in gradients. To compare the difference between the DLME loss and the CL loss, we assume that $g_\phi(\cdot)$ satisfies K -Lipschitz continuity [32], then

$$d_{ij}^z = k^* d_{ij}^y, k^* \in [1/K, K], \quad (9)$$

where k^* is a Lipschitz constant. The difference between CL loss and DLME loss is

$$|L_D - L_c| = \mathbb{E}_{x_j, x_j} \left[A_{ij} - \kappa \left((1 + (\alpha - 1) A_{ij}) k^* d_{ij}^z \right) \log \left(\frac{1}{\kappa(d_{ij}^z)} - 1 \right) \right] \quad (10)$$

The detailed derivation is provided in Appendix B. If i and j are neighbors, $A_{ij} = 1$, when $\alpha \rightarrow 0$, then $\alpha k^* d_{ij}^z \rightarrow 0$ and then $1 - \kappa(\alpha k^* d_{ij}^z) \rightarrow 0$, finally we have the $|L_D - L_c| \rightarrow 0$. When $\alpha \rightarrow 0$, the two losses have the same effect on the samples within each neighbor system. When $\alpha > 0$, the optimal solution of L_D retain a remainder about the embedding structure d_{ij}^z (in Appendix) which indicates that the DLME loss does not maximize the similarity of the neighborhood as the CL loss, but depends on the current embedding structure. Eq.(10) indicates that the DLME loss is smoother and can preserve the data structure in the embedding space. When $\alpha > 0$, the DLME loss is a smooth version of the CL loss, which causes minor collapse of local structures.

Generally, $f_\theta(\cdot)$ explores the structure of the prior manifolds defined by the given data augmentations smoothly, which can model the manifold structure more accurately than previous ML and DML methods.

3.4 Why DLME Leads to Local Flatness

This section discusses why the DLME loss optimizes the local curvature to be flatter. Network $f_\theta(\cdot)$ maps the data in the input space to the structure space for accurate structural modeling, although it is not guaranteed to obtain locally flat manifolds. Curling can cause overlap and deformation of the manifold, which can cause degradation of downstream task performance. To improve the performance in downstream tasks, we need to obtain an embedding space as flat as possible. The simplest linear methods can perform the discriminative tasks (classification, clustering, visualization).

DLME loss can enforce the flatness of the manifold in the embedded space. Similar to t-SNE, we use the kernel function of the long-tailed t-distribution to transform the distance metric into similarity. Further, we apply different ‘degrees of freedom’ parameters ν in the two latent spaces. The differences in the degree of freedom ν form two different kernel functions $\kappa(d, \nu^y)$ and $\kappa(d, \nu^z)$, and the difference of kernel functions will make the manifold in the embedding space flatter during the training process.

As described by Eq. (1), we use the local curvature description of the discrete surface to represent the flatness of the manifold. Next, we theoretically discuss why DLME’s loss can minimize the local curvature. We use the Push-pull property to describe the action of DLME loss on the embedding space.

Lemma 1 (Push-pull property). let $\nu^y > \nu^z$ and let $d^{z+} = \kappa^{-1}(\kappa(d, \nu^y), \nu^z)$ be the solution of minimizing L_D . Then exists d_p so that $(d^y - d_p)(d^{z+} - d^y) > 0$.

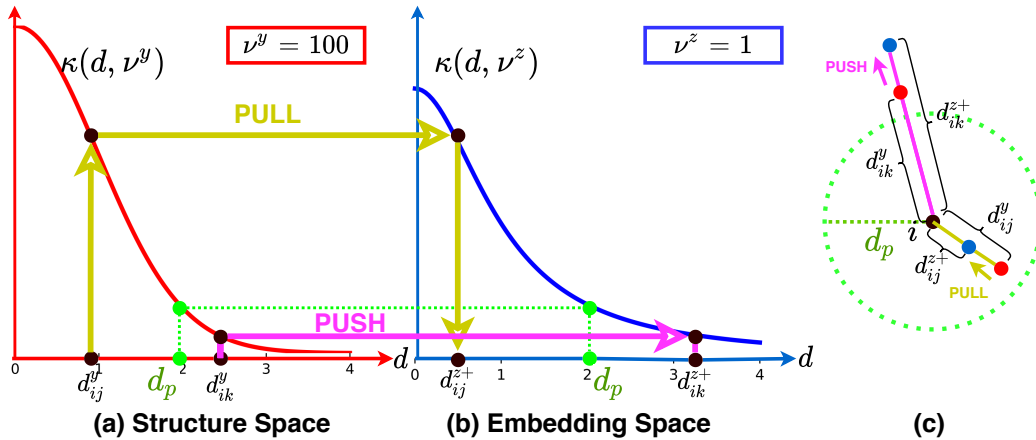


Figure 4: Push-pull property: if $d^y < d_p$ then $d^{z+} < d^y$ (in yellow), if $d^y > d_p$ then $d^{z+} > d^y$ (in pink).

The proof of lemma 1 is detailed in Appendix . Lemma 1 describes the push-pull property of the DLME loss between sample pairs in the embedding space. L_D decreases the distance between sample pairs within the threshold d_p (as similar pairs) and increases the distance between sample pairs beyond d_p (as dis-similar pairs), which shows pushing and pulling effects between two kinds of sample pairs.

Next, we prove that the DLME loss minimizes the average local curvature of the embedding based on the push-pull property.

Lemma 2. Assume $f_\theta(\cdot)$ satisfies HOP1-2 order preserving: $\max(\{d_{ij}^y\}_{j \in H_1(x_i)}) < \min(\{d_{ij}^z\}_{j \in H_2(x_i)})$ Then $\overline{K}_{\mathcal{M}}^{z+} < \overline{K}_{\mathcal{M}}^y$ where $\overline{K}_{\mathcal{M}}^y$ is the mean curvature in the structure space, and $\overline{K}_{\mathcal{M}}^{z+}$ is the mean curvature optimization results of L_D in the embedding space.

Lemma 2 indicates that the DLME loss encourages the flatness of the embedding space by decreasing the local average curvature. As Fig. 6, Lemma 2 describes that the optimization result of DLME loss is to flatten the manifold of the embedded space, which means that we can represent the data in a latent space as linear as possible.

DLME’s pseudo-code is shown in Algorithm 1.

Algorithm 1 The DLME algorithm

Input: Data: $\mathcal{X} = \{x_i\}_{i=1}^{|\mathcal{X}|}$, Learning rate: η , Epochs: E , Batch size: B , α, ν^y, ν^z , Network: f_θ, g_ϕ , **Output:** Graph Embedding: $\{e_i\}_{i=1}^{|\mathcal{X}|}$.

- 1: **while** $i = 0; i < E; i++$ **do**
- 2: $X^+ \leftarrow X \cup \tau(X)$. # data augmentation
- 3: **while** $b = 0; b < \lfloor |\mathcal{X}|/B \rfloor; b++$ **do**
- 4: $\{x_{a,1}, x_{a,2} \sim X^+\}_{a \in \mathcal{B}}, \mathcal{B} = \{1, \dots, B\}$; # sampling
- 5: $\{y_{a,0}, y_{a,1} \leftarrow f_\theta(x_{a,0}), f_\theta(x_{a,1})\}_{a \in \mathcal{B}}$; # map to \mathbb{R}^{d_y}
- 6: $\{z_{a,0}, z_{a,1} \leftarrow g_\phi(y_{a,0}), g_\phi(y_{a,1})\}_{a \in \mathcal{B}}$; # map to \mathbb{R}^{d_z}
- 7: $\{d_{a,ij}^y \leftarrow d(y_{a,0}, y_{a,1})\}_{a \in \mathcal{B}}; \{d_{a,ij}^z \leftarrow d(z_{a,0}, z_{a,1})\}_{a \in \mathcal{B}}$; #Cal. dist in \mathbb{R}^{d_y} & \mathbb{R}^{d_z}
- 8: $\{S_a^y \leftarrow \kappa(R(B_{a,ij}), d_{a,ij}^y, \nu^y)\}_{a \in \mathcal{B}}; \{S_a^z \leftarrow \kappa(d_{a,ij}^z, \nu^z)\}_{a \in \mathcal{B}}$; #Cal. sim in \mathbb{R}^{d_y} & \mathbb{R}^{d_z}
- 9: $\mathcal{L}_D \leftarrow E(\{D(S_a^y, S_a^z)\}_{a \in \mathcal{B}})$ by Eq. (4); # Cal. loss function
- 10: $\theta \leftarrow \theta - \eta \frac{\partial \mathcal{L}_D}{\partial \theta}, \phi \leftarrow \phi - \eta \frac{\partial \mathcal{L}_D}{\partial \phi}$; # update parameters
- 11: **end while**
- 12: **end while**
- 13: $\{z_i \leftarrow f_\theta(g_\phi(x_i))\}_{i \in \{1, 2, \dots, \mathcal{X}\}}$; # Cal. the embedding result

4 Experiments

In this section, we evaluate the effectiveness of the proposed DLME on four downstream tasks (classification/linear test, clustering, visualization) and analyze each proposed component with the following questions.

- (Q1) How to intuitively understand structural distortions?
- (Q2) Does DLME overcome structural distortions?
- (Q3) How to intuitively understand underconstrained manifold embedding?
- (Q4) Does DLME overcome underconstrained manifold embedding and obtain locally flat embeddings?
- (Q5) How much does DLME improve the performance of downstream tasks on ML and CL datasets?
- (Q6) Can smoother losses bring better performance to CL?

4.1 Visualization of Structural Distortions (Q1,Q2)

Experimental setups. This section illustrates structural distortions on image datasets and experimentally demonstrates that DLME can overcome structural distortions by introducing prior knowledge of data augmentation. In this experiment, all the data are mapped to a 2-D latent space to facilitate the visualization. All compared ML methods (t-SNE, PUMAP, ivis, and PHA) will fail in the CIFAR dataset; we only show the results of UMAP.

Structural Distortions. ML methods model structure using distance metrics from observations. Complex data (increasing dimensionality and decreasing sampling) leads to the failure of the distance metric, confusing semantic nearest neighbors, which subsequently destroys local connectivity and eventually produces structural distortions in the ML process. DLME constructs a smoother CL framework with the help of data augmentation. The proposed framework

obtains richer prior knowledge with data augmentation. It maps the data into the latent space for structural modeling with neural networks, which can achieve more accurate modeling and thus overcome structural distortion.

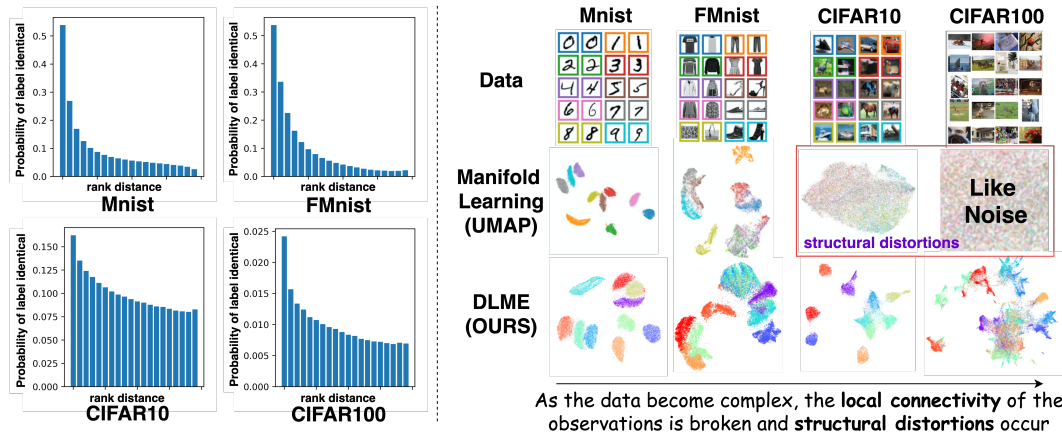


Figure 5: (left) Barplot of probabilities of label identical vs rank distance. A higher left end of barplot indicates a higher probability of the same label for the nearest neighbor sample, implying that local connectivity is guaranteed. (right) Results of ML method (UMAP) on four image datasets. Local connectivity cannot be guaranteed for complex data, causing ML method embedding to fail. The proposed DLME method has better embedding results on the more complex CIFAR dataset.

4.2 Visualization of Underconstrained Manifold Embedding (Q3,Q4)

This section illustrates underconstrained manifold embedding with toy datasets and experimentally demonstrates the DLME potential to solve this problem by constraining the local curvature.

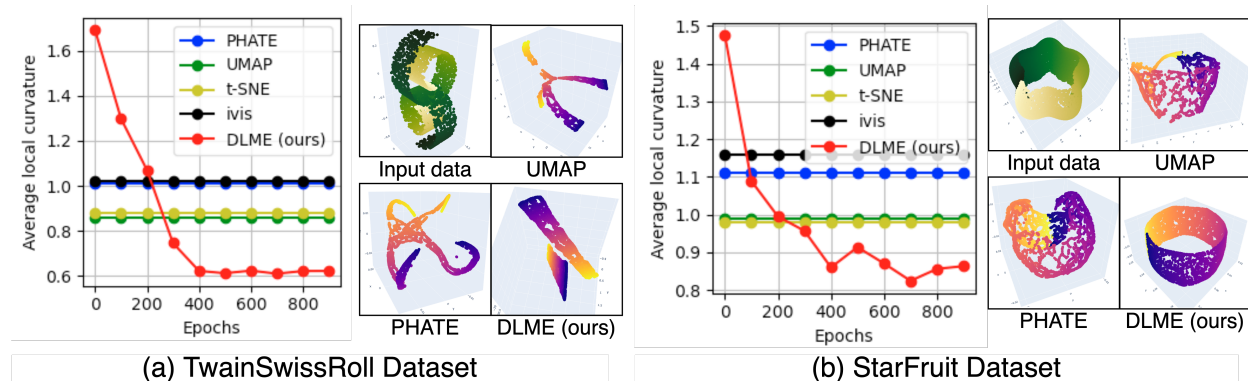


Figure 6: Average local curvature and scatter plot on TwainSwissRoll and StarFruit dataset. The two examples indicate that traditional ML produces distorted embeddings, which affect the performance of downstream tasks. In contrast, DLME can get as flat embeddings as possible by optimizing the local curvature.

Experimental setups. We used two 3D toy datasets, TwainSwissRoll and StarFruit. TwainSwissRoll: two entwined but non-intersecting SwissRoll. StarFruit: locally curved surface. The 3D embeddings of ML methods are in Fig. 6. The results are in Fig. 6, and the detailed results are in Appendix . The details of dataset is in Appendix .

Underconstrained manifold embedding. The results in Fig. 6 show that the compared ML methods produce bends that should not exist. We attribute these bends to inadequate constraints on the loss function. These bends can affect the effectiveness of downstream tasks (e.g., classification, clustering, etc.). The more complex and heterogeneous data can cause more significant damage than the toy dataset.

Benefits of local flat embedding. DLME tries to obtain a locally flat embedding based on the local flatness assumption. The statistics of the average curvature show that DLME can obtain a flatter local flow shape. We argue that a flat

Table 1: Performance comparison on 12 datasets. **Bold** denotes the best result and Underline denotes 5% higher than others.

	Classification Accuracy (linear SVM)						Clustering Accuracy (K-means)					
	tSNE	UMAP	PUMAP	ivis	PHA	DLME	tSNE	UMAP	PUMAP	ivis	PHA	DLME
Digits	0.949	0.960	0.837	0.767	0.928	0.973	0.938	0.875	0.763	0.726	0.794	0.956
Coil20	0.799	0.834	0.774	0.672	0.828	0.909	0.763	0.821	0.722	0.612	0.655	0.899
Coil100	0.760	0.756	N/A	0.542	0.653	0.952	0.763	0.785	N/A	0.492	0.515	0.944
Mnist	0.963	0.966	0.941	0.671	0.796	0.976	0.904	0.801	0.772	0.466	0.614	0.977
EMnist	0.420	0.588	0.384	0.190	0.416	0.657	0.478	0.537	0.363	0.178	0.352	0.641
KMnist	0.738	0.656	0.674	0.547	0.607	0.782	0.586	0.668	0.706	0.522	0.594	0.712
Colon	0.932	0.893	0.918	0.942	0.930	0.947	0.862	0.847	0.861	0.922	0.855	0.924
Activity	0.861	0.844	0.849	0.831	0.798	0.921	0.784	0.639	0.783	0.681	0.679	0.898
MCA	0.719	0.675	0.667	0.634	0.552	0.774	0.475	0.532	0.464	0.443	0.414	0.563
Gast10k	0.821	0.846	0.706	0.687	0.676	0.918	0.534	0.546	0.512	0.427	0.523	0.598
SAMUSIK	0.556	0.678	0.599	0.625	0.675	0.700	0.335	0.387	0.345	0.328	0.511	0.572
HCL	0.884	0.863	0.767	0.454	0.393	0.884	0.689	0.743	0.619	0.308	0.263	0.753

embedding possesses practical benefits, such as a flatter local manifold can achieve better performance in downstream tasks and is more suitable for interpretability analysis of deep models. For example, it is easy to distinguish two sub-manifolds of TwainSwissRoll using a linear classifier, and it is easy to perform regression tasks on StarFruit.

4.3 Comparison on Traditional ML Datasets (Q5, Q6)

Experimental setups: The compared methods include two ML methods (UMAP [6], t-SNE [33]) and three deep ML methods (PHATE [34], ivis [20] and parametric UMAP (PUMAP) [18].) The datasets include six image datasets (Digits, Coil20, Coil100, Mnist, EMnist, and KMnist) and six biological datasets (Colon, Activity, MCA, Gast10k, SAMUSIK, and HCL60K). We map data into a 2-D space and then evaluate them by 10-fold cross-validation. We use a linear SVM and k-means to test the accuracy of in the latent space as performance, and the results are in Table 1. The MLP architecture of f_θ is [-1,500,300,80], where -1 is the dimension of input data. The MLP architecture of g_ϕ is [80,500,80,2]. Details of datasets, baseline methods, and evaluation metrics are in Appendix .

Analyse: DLME has advantages over all 12 datasets, and DLME is 5% higher than other methods in 14 items (24 items in total). The experimental results show that DLME has advantages in classification and clustering metrics. We summarize the reasons why DLME has performance advantages as follows. (1) Compared with ML methods, DLME overcomes structural distortions to a certain extent to model the structure more accurately. (2) DLME reduces the overlap of different clusters, improving the performance of classification and clustering. (3) The locally flat embeddings learned by DLME are linearly characterized and more suitable for the linear model.

4.4 Comparison on CL Datasets (Q5, Q6)

Table 2: The linear-test performance.						Table 3: The clustering performance.					
	CF10	CF100	STL10	TINet	IN100	Dataset	CF10	CF100	STL10	TINet	IN-Dog
NPID	0.827	0.571	0.825	0.382	0.721	DAC	0.522	0.238	0.470	0.066	0.219
ODC	0.799	0.521	0.734	0.287	0.645	DCCM	0.623	0.327	0.482	0.108	0.321
SimCLR	0.882	0.574	0.869	0.384	0.756	PICA	0.696	0.337	0.713	0.098	0.352
MoCo.v2	0.886	0.614	0.856	0.374	0.780	CC	0.747	0.429	0.850	0.140	0.445
BYOL	0.881	0.644	0.887	0.388	0.785	CRLC	0.799	0.425	0.818	0.153	0.461
DLME	0.913	0.661	0.901	0.449	0.793	DLME	0.822	0.441	0.883	0.182	0.483
DLME-A1	0.910	0.653	0.881	0.428	0.785	DLME-A1	0.792	0.417	0.872	0.145	0.479
DLME-A2	0.902	0.626	0.879	0.432	0.791	DLME-A2	0.783	0.421	0.859	0.133	0.480
DLME-A3	0.888	0.624	0.873	0.401	0.783	DLME-A3	0.779	0.417	0.852	0.134	0.477

Experimental setups: Due to structural distortions, ML methods fail in CV Datasets, and our comparison is limited to the CL and deep clustering (DC) domain. The compared methods include CL methods (NPID [21], ODC [35], SimCLR [8], MOCO.v2 [9] and BYOL [10]) and deep clustering methods (DAC [36], DDC [37], DCCM [38], PICA

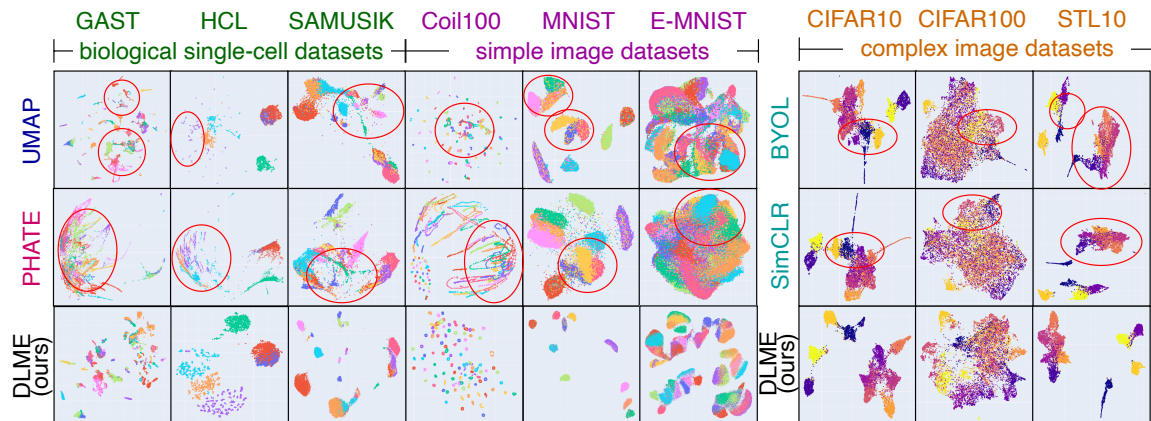


Figure 7: Visualization results of biological datasets, simple image datasets and complex image datasets. The red circle indicates the clusters confused by the baseline method.

[39], CC [40], and CRLC [41]). The datasets include six image datasets: CIFAR10 (CF10), CIFAR100 (CF100), STL10, TinyImageNet (TINet), ImageNet-Dog (IN-DOG) and ImageNet100 (IN100)). The f_θ is ResNet50, and g_ϕ is MLP with architecture of [2048, 256]. We use the same settings as SimCLR for the linear test and use the same settings as CC[40] for deep clustering. The results are in Table 2 and Table 3 and the detailed setup is in Appendix .

Analyse: DLME outperforms these SOTA methods by a large margin on all datasets. And it is 2% higher than other methods in 6 items (10 items in total). The reasons why DLME has advantages in linear-test and clustering tasks are summarized as follows: (1) Compared with the CL method, the DLME framework is smoother and avoids problems such as falling into local collapse. (2) The locally flat embeddings learned by DLME are linearly characterized and more suitable for a linear model.

Ablation Study. We designed ablation experiments to demonstrate the effectiveness of DLME. **Ablation 1 (DLME-A1):** We detach the L_D 's gradient on the model $f_\theta(\cdot)$ and replace it with the CL loss (in Eq. (8)). The model is divided into two separate parts. One obtains embedding with CL, and the other emphasizes the flatness of manifold with similarity loss. **Ablation 2 (DLME-A2):** Based on DLME-A1, We ablate the t-distribution kernel and use a standard distribution kernel in both spaces. **Ablation 3 (DLME-A3):** Finally, we further ablate the structure of the two networks and transform the model into a CL method. The results of ablation experiments are in Table 2 and Table 3. The experimental results show that the three critical operations of DLME can improve the performance in complex manifold embedding tasks.

4.5 Visualization of ML and CV Datasets (Q5, Q6)

The visualization task is a particular embedding task. With the help of visualization, we can intuitively analyze the performance of methods. The visualization results of all data sets are in Appendix . As the selected visualization results are shown in Fig. 7, DLME significantly outperforms other methods in terms of visualization results. Because the distortion problem is overcome, the DLME embedding results in a minimum mixture of different clusters with clear boundaries.

5 Conclusion

Structural and distributional distortions limit the performance of ML. To this end, we propose Deep Local-flatness Manifold Embedding (DLME), a novel ML framework to obtain reliable manifold embedding by reducing distortion. In the experiments, by demonstrating the effectiveness of DLME on downstream classification, clustering, and visualization tasks with three types of datasets (toy, biological, and image), our experimental results show that DLME outperforms SOTA ML & CL methods.

Acknowledgement

This work is supported by National Natural Science Foundation of China, named Geometric Deep Learning and Applications in Proteomics-Based Cancer Diagnosis (No. U21A20427). This work is supported by Alibaba Innovative Research (AIR) Programme.

References

- [1] Tune H Pers, Anders Albrechtsen, Claus Holst, Thorkild IA Sørensen, and Thomas A Gerds. The validation and assessment of machine learning: a game of prediction from high-dimensional data. *PLoS One*, 4(8):e6287, 2009.
- [2] Rakesh Agrawal, Johannes Gehrke, Dimitrios Gunopulos, and Prabhakar Raghavan. Automatic subspace clustering of high dimensional data for data mining applications. In *Proceedings of the 1998 ACM SIGMOD international conference on Management of data*, pages 94–105, 1998.
- [3] David L Donoho et al. High-dimensional data analysis: The curses and blessings of dimensionality. *AMS math challenges lecture*, 1(2000):32, 2000.
- [4] Dmitry Kobak and George C Linderman. Umap does not preserve global structure any better than t-sne when using the same initialization. *BioRxiv*, 2019.
- [5] Dmitry Kobak and George C Linderman. Initialization is critical for preserving global data structure in both t-sne and umap. *Nature biotechnology*, 39(2):156–157, 2021.
- [6] Leland McInnes, John Healy, and James Melville. UMAP: Uniform Manifold Approximation and Projection for Dimension Reduction. *arXiv:1802.03426 [cs, stat]*, February 2018. arXiv: 1802.03426 version: 1.
- [7] Laurens van der Maaten and Geoffrey Hinton. Visualizing data using t-SNE. *Journal of machine learning research*, 9(Nov):2579–2605, 2008.
- [8] Ting Chen, Simon Kornblith, Mohammad Norouzi, and Geoffrey Hinton. A Simple Framework for Contrastive Learning of Visual Representations. *arXiv:2002.05709 [cs, stat]*, June 2020. arXiv: 2002.05709.
- [9] Kaiming He, Haoqi Fan, Yuxin Wu, Saining Xie, and Ross Girshick. Momentum Contrast for Unsupervised Visual Representation Learning. *arXiv:1911.05722 [cs]*, March 2020. arXiv: 1911.05722.
- [10] Jean-Bastien Grill, Florian Strub, Florent Alché, Corentin Tallec, Pierre H. Richemond, Elena Buchatskaya, Carl Doersch, Bernardo Avila Pires, Zhaohan Daniel Guo, Mohammad Gheshlaghi Azar, Bilal Piot, Koray Kavukcuoglu, Rémi Munos, and Michal Valko. Bootstrap Your Own Latent: A New Approach to Self-Supervised Learning. *arXiv:2006.07733 [cs, stat]*, June 2020. arXiv: 2006.07733.
- [11] Lilian Weng. Contrastive representation learning. *lilianweng.github.io*, 2021.
- [12] Jure Zbontar, Li Jing, Ishan Misra, Yann LeCun, and Stéphane Deny. Barlow twins: Self-supervised learning via redundancy reduction. In *International Conference on Machine Learning*, pages 12310–12320. PMLR, 2021.
- [13] Joseph B Kruskal. Nonmetric multidimensional scaling: a numerical method. *Psychometrika*, 29(2):115–129, 1964.
- [14] J. B. Tenenbaum. A Global Geometric Framework for Nonlinear Dimensionality Reduction. *Science*, 290(5500):2319–2323, December 2000.
- [15] Sam T Roweis and Lawrence K Saul. Nonlinear dimensionality reduction by locally linear embedding. *science*, 290(5500):2323–2326, 2000. Publisher: American Association for the Advancement of Science.
- [16] Geoffrey E. Hinton and Sam T. Roweis. Stochastic neighbor embedding. In *Advances in neural information processing systems*, pages 857–864, 2003.
- [17] Laurens van der Maaten. Learning a Parametric Embedding by Preserving Local Structure. In *Artificial Intelligence and Statistics*, pages 384–391. PMLR, April 2009. ISSN: 1938-7228.
- [18] Tim Sainburg, Leland McInnes, and Timothy Q. Gentner. Parametric UMAP embeddings for representation and semi-supervised learning. *arXiv:2009.12981 [cs, q-bio, stat]*, April 2021. arXiv: 2009.12981.
- [19] Andres F. Duque, Sacha Morin, Guy Wolf, and Kevin Moon. Extendable and invertible manifold learning with geometry regularized autoencoders. *2020 IEEE International Conference on Big Data (Big Data)*, Dec 2020.
- [20] Benjamin Szubert, Jennifer E. Cole, Claudia Monaco, and Ignat Drozdov. Structure-preserving visualisation of high dimensional single-cell datasets. *Scientific Reports*, 9(1):8914, June 2019.
- [21] Zhirong Wu, Yuanjun Xiong, Stella Yu, and Dahua Lin. Unsupervised Feature Learning via Non-Parametric Instance-level Discrimination. *arXiv:1805.01978 [cs]*, May 2018. arXiv: 1805.01978.
- [22] John Nash. The imbedding problem for riemannian manifolds. *Annals of mathematics*, pages 20–63, 1956.
- [23] Sam T Roweis and Lawrence K Saul. Nonlinear dimensionality reduction by locally linear embedding. *science*, 290(5500):2323–2326, 2000.
- [24] Ichirō Satake. The gauss-bonnet theorem for v-manifolds. *Journal of the Mathematical Society of Japan*, 9(4):464–492, 1957.

- [25] John Harer and Don Zagier. The euler characteristic of the moduli space of curves. *Inventiones mathematicae*, 85(3):457–485, 1986.
- [26] Emmanuel J Candès and Michael B Wakin. An introduction to compressive sampling. *IEEE signal processing magazine*, 25(2):21–30, 2008.
- [27] Xiaohang Zhan, Jiahao Xie, Ziwei Liu, Yew-Soon Ong, and Chen Change Loy. Online deep clustering for unsupervised representation learning. In *Proceedings of the IEEE/CVF Conference on Computer Vision and Pattern Recognition*, pages 6688–6697, 2020.
- [28] Bo Cheng, Wanyin Wu, Dapeng Tao, Shibo Mei, Ting Mao, and Jun Cheng. Random cropping ensemble neural network for image classification in a robotic arm grasping system. *IEEE Transactions on Instrumentation and Measurement*, 69(9):6795–6806, 2020.
- [29] Jan Flusser, Sajad Farokhi, Cyril Höschl, Tomáš Suk, Barbara Zitova, and Matteo Pedone. Recognition of images degraded by gaussian blur. *IEEE transactions on Image Processing*, 25(2):790–806, 2015.
- [30] Stan Z Li, Zelin Zang, and Lirong Wu. Deep manifold transformation for dimension reduction. *arXiv preprint arXiv:2010.14831*, 2020.
- [31] Irmgard Flugge-Lotz. *Discontinuous automatic control*. Princeton University Press, 2015.
- [32] Henry Gouk, Eibe Frank, Bernhard Pfahringer, and Michael Cree. Regularisation of Neural Networks by Enforcing Lipschitz Continuity. *arXiv:1804.04368 [cs, stat]*, September 2018. arXiv: 1804.04368.
- [33] G. E. Hinton and R. R. Salakhutdinov. Reducing the dimensionality of data with neural networks. *Science*, 313(5786):504–507, 2006.
- [34] Kevin R Moon and van Dijk. Visualizing structure and transitions in high dimensional biological data. *Nature biotechnology*, 37(12):1482–1492, 2019.
- [35] Xiaohang Zhan, Jiahao Xie, Ziwei Liu, Yew-Soon Ong, and Chen Change Loy. Online Deep Clustering for Unsupervised Representation Learning. In *2020 IEEE/CVF Conference on Computer Vision and Pattern Recognition (CVPR)*, pages 6687–6696, Seattle, WA, USA, June 2020. IEEE.
- [36] Philip Haeusser, Johannes Plapp, Vladimir Golkov, Elie Aljalbout, and Daniel Cremers. Associative Deep Clustering: Training a Classification Network with No Labels. In Thomas Brox, Andrés Bruhn, and Mario Fritz, editors, *Pattern Recognition*, pages 18–32. Springer International Publishing, 2019.
- [37] Jianlong Chang, Yiwen Guo, Lingfeng Wang, Gaofeng Meng, Shiming Xiang, and Chunhong Pan. Deep Discriminative Clustering Analysis. *arXiv:1905.01681 [cs, stat]*, May 2019. arXiv: 1905.01681.
- [38] Jianlong Wu, Keyu Long, Fei Wang, Chen Qian, Cheng Li, Zhouchen Lin, and Hongbin Zha. Deep Comprehensive Correlation Mining for Image Clustering. pages 8150–8159, 2019.
- [39] Jiabo Huang, Shaogang Gong, and Xiatian Zhu. Deep Semantic Clustering by Partition Confidence Maximisation. pages 8849–8858, 2020.
- [40] Yunfan Li, Peng Hu, Zitao Liu, Dezhong Peng, Joey Tianyi Zhou, and Xi Peng. Contrastive Clustering. *AAAI2021*, September 2021. arXiv: 2009.09687.
- [41] Kien Do, Truyen Tran, and Svetha Venkatesh. Clustering by maximizing mutual information across views, 2021.